scientific reports

Check for updates

OPEN

Nonlinear optical property measurements of rhenium diselenide used for ultrafast fiber laser mode-locking at 1.9 μm

Jinho Lee[1], Suhyoung Kwon[1], Taeyoon Kim[1], Junha Jung[1], Luming Zhao[2] & Ju Han Lee[1,3]✉

An experimental investigation into the nonlinear optical properties of rhenium diselenide ($ReSe_2$) was conducted at a wavelength of 1.9 μm using the open-aperture and closed-aperture Z-scan techniques for the nonlinear optical coefficient (β) and nonlinear refractive index (n_2) of $ReSe_2$, respectively. β and n_2 measured at 1.9 μm were ~ -11.3×10^3 cm/GW and ~ -6.2×10^{-2} cm^2/GW, respectively, which to the best of our knowledge, are the first reported measurements for $ReSe_2$ in the 1.9-μm spectral region. The electronic band structures of both $ReSe_2$ and its defective structures were also calculated via the Perdew–Becke–Erzenhof functional to better understand their absorption properties. A saturable absorber (SA) was subsequently fabricated to demonstrate the usefulness of $ReSe_2$ for implementing a practical nonlinear optical device at 1.9 μm. The 1.9-μm SA exhibited a modulation depth of ~ 8% and saturation intensity of ~ 11.4 MW/cm^2. The successful use of the $ReSe_2$-based SA for mode-locking of a thulium–holmium (Tm–Ho) co-doped fiber ring cavity was achieved with output pulses of ~ 840 fs at 1927 nm. We believe that the mode-locking was achieved through a hybrid mechanism of saturable absorption and nonlinear polarization rotation.

Nonlinear optical materials have been an essential part of realizing various nonlinear functions in optical and photonic devices, such as frequency conversion[1,2], parametric processes[3], optical switching[4], and saturable absorption[5]. The aforementioned nonlinear optical functions require different nonlinear optical effects of the material; for example, the $\chi^{(2)}$ effect is used for the implementation of optical wavelength converters[6], $\chi^{(3)}$ is for optical switches[7], and nonlinear absorption is for saturable absorbers (SAs)[8].

SAs can be broadly categorized into fast and slow devices. It is well-known that fast SAs are suitable for generating ultrashort pulses owing to their immediate response time[9]. Optical fiber-based nonlinear transmission devices comprising a nonlinear optical loop mirror (NOLM), a nonlinear amplifying loop mirror, or nonlinear polarization rotation (NPR) are commonly known as fast SAs[10–12]. However, mode-locking with the aforementioned optical fiber-based nonlinear devices has a self-starting difficulty. On the other hand, one of the latest developments in the field of materials science, nonlinear saturable absorption materials, are known to be relatively slow SAs compared to optical fiber-based nonlinear transmission devices. The saturable absorption phenomenon usually occurs because of Pauli's blocking principle within semiconductors[13]. It is well-known that nonlinear material-based SAs are suitable for self-starting mode-locking operations. Until now, many nonlinear optical materials can be used as relatively slow SAs, such as carbon nanotubes[5,14,15], graphene[8,16,17], topological insulators (TIs)[18,19], transition metal dichalcogenides (TMDCs)[20–25], lead sulfide (PbS)[26], and MXenes[27–29].

Hybrid mode-locking techniques have been widely investigated to solve the difficulty with self-starting for conventional mode-locking in optical fiber-based nonlinear transmission devices. They can induce self-starting mode-locking with ultrafast and stable pulses by combining an optical fiber-based nonlinear transmission device and a nonlinear material-based SA: the former can induce ultrashort pulse duration while the latter can easily initiate self-starting for the mode-locking process to enhance the overall mode-locking stability.

Among the saturable absorption materials, TMDCs have received much attention. TMDCs have the chemical formula MX_2 (M: transition metal, X: chalcogen). Zhang et al.[20] first investigated the saturable absorption

[1]School of Electrical and Computer Engineering, University of Seoul, Seoul 02504, South Korea. [2]School of Optical and Electronic Information and Wuhan National Laboratory for Optoelectronics, Huazhong University of Science and Technology, Wuhan 430074, China. [3]Institute of Information Technology, University of Seoul, Seoul 02504, South Korea. ✉email: j.h.lee@ieee.org

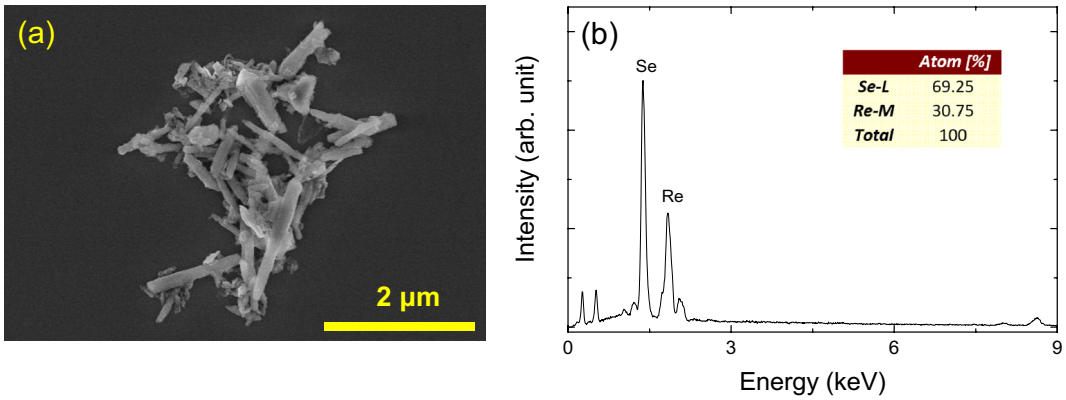

Figure 1. (**a**) An SEM image and (**b**) an EDS spectrum of $ReSe_2$ particles.

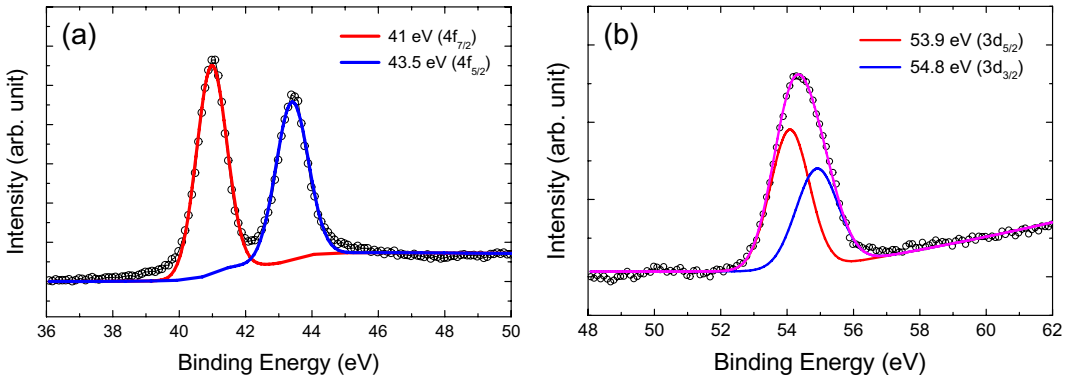

Figure 2. XPS core-level spectra: (**a**) Re 4f and (**b**) Se 3d.

property of molybdenum disulfide (MoS_2), after which this property has been extensively investigated in various other TMDCs[20–25].

Compared to conventional group VI TMDCs (molybdenum- or tungsten-based ones), rhenium-based ones (group VII TMDCs) are known to possess quite different optical and electronic characteristics. Very recently, several rhenium-based TDMCs, such as rhenium disulfide (ReS_2) and $ReSe_2$, for use as nonlinear SAs have been reported[30–34]. These SAs have been implemented in Q-switching[31,32] or mode-locking[33,34], and their nonlinear absorption coefficients have been obtained using Z-scan techniques conducted at wavelengths of 515, 1030, or 1560 nm[33,34].

In this work, we measured the nonlinear optical properties of $ReSe_2$ at a wavelength of 1.9 μm. First, the nonlinear absorption coefficient (β) of $ReSe_2$ was measured using the open-aperture (OA) Z-scan technique (~ − 11.3 × 10^3 cm/GW). Next, the nonlinear refractive index (n_2) of $ReSe_2$ was measured using the closed-aperture (CA) Z-scan technique (~ − 6.2 × 10^{-2} cm^2/GW). To the best of our knowledge, these are the first measurements of β and n_2 of $ReSe_2$ in the 1.9-μm spectral region. Density functional theory (DFT) calculations were conducted to determine the electronic band structures of $ReSe_2$ for different ratios of Re and Se atoms. Finally, a composite of $ReSe_2$ and polyvinyl alcohol (PVA) was fabricated to assess the practicability of using $ReSe_2$ as an SA at 1.9 μm. Ultrafast ~ 840 fs pulses could readily be obtained after incorporating the prepared SA into a 1.9 μm fiber ring cavity as a mode-locker.

Results

Material characterization and bandgap calculation of $ReSe_2$ particles. $ReSe_2$ bulk flakes were first suspended in 10 mL distilled water, after which the solution was sonicated for 16 h to obtain nano-sized particles. Scanning electron microscopy (SEM) was conducted on the sonicated particles, and the SEM image in Fig. 1a clearly illustrates that the particle size varied from hundreds of nanometers to a few micrometers, indicating that the $ReSe_2$ particles were still in the bulk state.

Characterization of the sonicated $ReSe_2$ particles was conducted via energy dispersive spectroscopy (EDS). From the two distinct peaks corresponding to Re and Se can be clearly observed in the EDS spectrum in Fig. 1b, the atomic ratio between Re and Se was 1:2. Stoichiometric analysis of the $ReSe_2$ particles was performed via X-ray photoelectron spectroscopy (XPS). The two peaks in the Re $4f_{7/2}$ and Re $4f_{5/2}$ spectra (Fig. 2a) at ~ 41 and ~ 43.5 eV, respectively, are consistent with previously reported values[35,36], while two peaks at ~ 53.9 and ~ 54.8 eV in the Se 3d spectrum (Fig. 2b) signify the presence of Se $3d_{5/2}$ and Se $3d_{3/2}$[35,36], respectively.

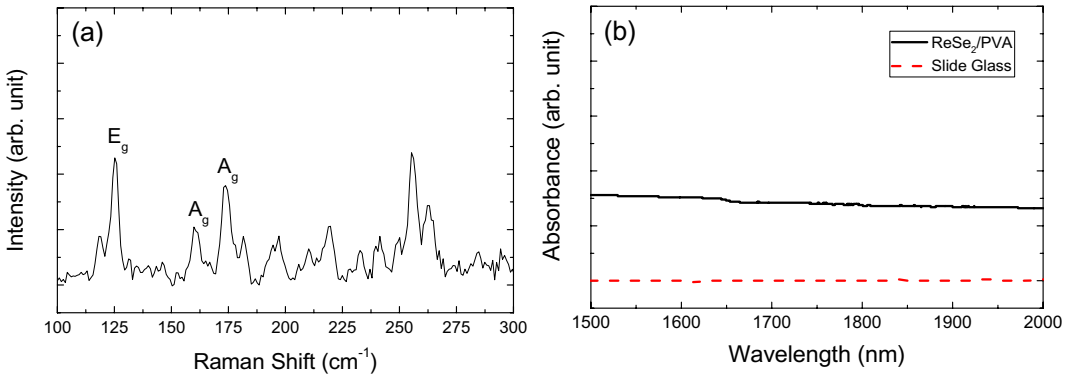

Figure 3. (**a**) A Raman spectrum of the $ReSe_2$ particles and (**b**) measured linear absorption spectrum of the $ReSe_2$/PVA film.

Raman spectroscopy (Fig. 3a) revealed three peaks corresponding to the E_g (~ 125 cm^{-1}) and A_g (~ 160 cm^{-1} and ~ 173.7 cm^{-1}) modes. Many other small peaks in the spectrum can be attributed to the low lattice symmetry and complex lattice vibrations of the particles[35–39]. The size of the $ReSe_2$ particles used in this experimental investigation ranged from tens of nanometers to a few micrometers rather than just a few layered evenly sized nanoparticles. To enable the facile formation of a thin film, we combined the $ReSe_2$ solution with polyvinyl alcohol (PVA). The $ReSe_2$/PVA composite film was then characterized via linear optical absorption (Shimadzu, UV-3600PLUS) measurements after the $ReSe_2$/PVA solution had been dropped onto a glass slide and then dried for 1 hour. As shown in Fig. 3b, it is clear that the prepared film had wide spectral band absorption.

To better understand the electronic band structures of $ReSe_2$, first-principle calculations were performed using the Quantum Espresso package (Materials square)[40]. We conducted the simulation with different ratios (R) of Re and Se atoms (1:2, 1:1.75, and 1:2.667) for which the Perdew–Becke–Erzenhof (PBE) functional was adopted and cutoff-energy of 30 Ry and the ultrasoft pseudopotential were applied. As shown in Fig. 4a, pristine $ReSe_2$ with no vacancy has a bandgap of ~ 1.24 eV, which is in good agreement with previously reported values[33,38]. However, the bandgaps of defective $ReSe_2$ structures were also calculated with R = 1:1.75 and 1:2.667, as shown in Fig. 4b,c. The indirect bandgap of ~ 0.26 eV, which corresponds to a cut-off wavelength of ~ 4.7 μm, was estimated for R = 1:1.75 whereas a metallic band structure was obtained for R = 1:2.667. These simulation results indicate that the bandgap of $ReSe_2$ decreases with an increase in the atomic defect, thereby enabling a broader saturable absorption bandwidth including the mid-infrared wavelength region. A decrease in the defect-induced energy bandgap in TMDC materials has been reported previously[33,41–43], and the oxidation and defects of TMDCs do not degrade their saturable absorption properties[19,43]. Thus, we can infer that the stability of materials in terms of saturable absorption is not related to oxidation and defects.

Nonlinear optical property measurements using Z-scan techniques. The nonlinear optical properties of the $ReSe_2$ particles were studied via the Z-scan techniques[44]. Figure 5 shows the Z-scan measurement setup, in which a ~ 550-fs pulsed fiber laser was employed as the input beam. A $ReSe_2$/PVA film was vertically placed on the translation stage with a laser output beam focused through the lens onto the film, after which the sample position was moved from z = − 20 to 20 mm. The $ReSe_2$/PVA film exhibited an obvious nonlinear saturable absorption response (Fig. 6a); as z approaches 0 (the intensity of the incident beam increased), the normalized transmission was observed to monotonically increase. The transmittance change of the $ReSe_2$/PVA film was monitored with a power meter. The normalized transmittance ($T(z)$) of the measured graph was plotted along the z position with a fitted curve based on the following formula[45]:

$$T(z) = \sum_{n=0}^{\infty} (-\beta I_0 L_{eff})^n / (1 + z^2/z_0^2)^n (n+1)^{3/2} \approx 1 - \beta I_0 L_{eff} / 2^{3/2} (1 + z^2/z_0^2), \quad (1)$$

$$L_{eff} = (1 - e^{-\alpha_0 L})/\alpha_0, \quad (2)$$

where β represents the nonlinear absorption coefficient; I_0 is the peak intensity at the focusing point; α_0 denotes the linear absorption coefficient; z and z_0 denote the position of the film and the Rayleigh length, respectively; L represents the film thickness.

We subsequently conducted a CA Z-scan analysis to measure the nonlinear refractive index of the $ReSe_2$/PVA film; Fig. 6b shows the Z-scan results as a fitted curve based on the following formula[46]:

$$T(z) = \frac{1}{1 - \frac{4z/z_0}{(1+z^2/z_0^2)^2}\Delta\Phi + \frac{4}{(1+z^2/z_0^2)^3}\Delta\Phi^2}, \quad (3)$$

$$\Delta\Phi = 2\pi n_2 I_0 L_{eff}/\lambda, \quad (4)$$

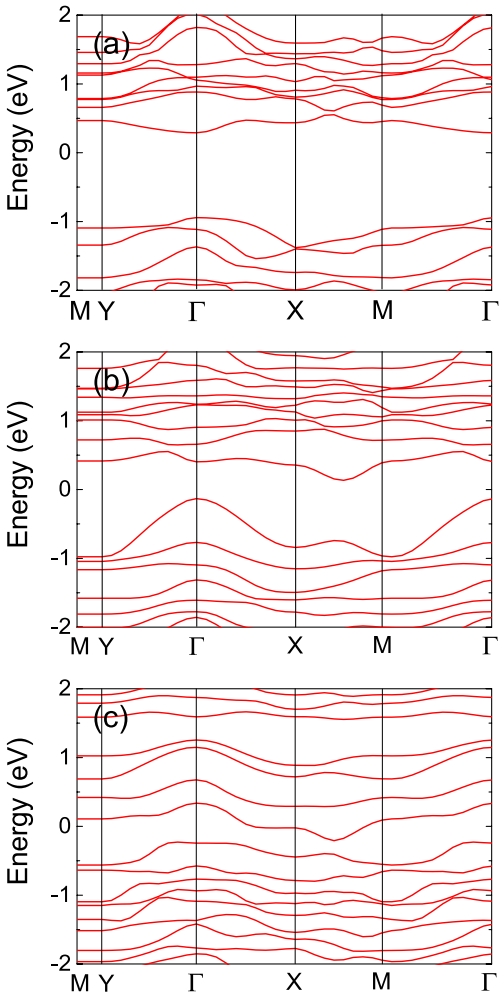

Figure 4. Calculated electronic band structures of $ReSe_2$ with (**a**) R = 1:2, (**b**) R = 1:1.75, and (**c**) R = 1:2.667.

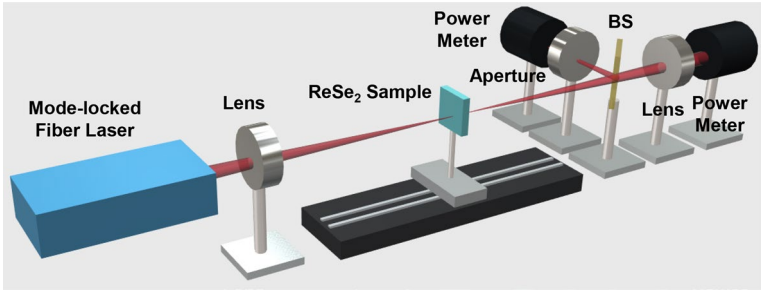

Figure 5. Measured setup for the Z-scan measurements.

$$z_0 = \pi\omega_0^2/\lambda, \tag{5}$$

where ω_0 is the beam waist, λ is the light wavelength, and n_2 denotes the nonlinear refractive index.

From the measurement results and fitted curves (Fig. 6), the nonlinear absorption coefficient of the $ReSe_2$/PVA film was estimated as $\sim -11.3 \times 10^3$ cm/GW and its refractive index was $\sim -6.2 \times 10^{-2}$ cm^2/GW at 1.9 μm. For comparison, the reported nonlinear optical parameters for several other TMDCs are listed in Table 1. Nevertheless, it was not possible to directly compare the measured parameters of $ReSe_2$ with the ones of other TMDCs because, to the best of our knowledge, no previous measurements of the nonlinear optical parameters for TMDCs in the 2-μm wavelength area have been reported. The nonlinear absorption coefficient and nonlinear refractive index of $ReSe_2$ at 1.9 μm are twice as larger as the values at 1560 nm[34]. In our previous work, we

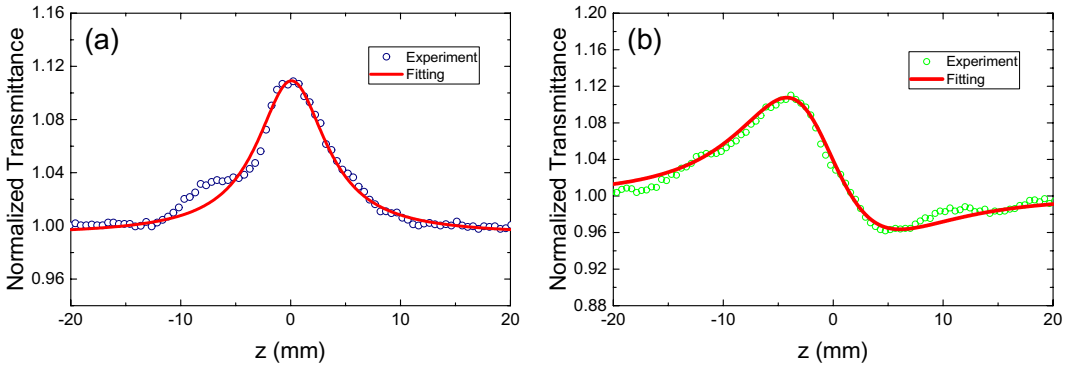

Figure 6. Plots for the (**a**) open-aperture and (**b**) closed aperture Z-scans of the $ReSe_2$ film.

TMDC materials	λ (nm)	α_0 (cm^{-1})	β (cm/GW)	n_2 (cm^2/GW)	Refs.
Monolayer MoS_2	532	NA[a]	-10.11×10^5	NA	[54]
Monolayer MoS_2	532	NA	-7.24×10^5	NA	[54]
Monolayer MoS_2	532	NA	-1.67×10^5	NA	[54]
Monolayer MoS_2	532	NA	0.22×10^5	NA	[54]
MoS_2	800	5.4×10^4	− 136.13	NA	[55]
MoS_2 (25–27 L)	800	6.24×10^4	11.4 ± 4.3	NA	[56]
MoS_2 (25–27 L)	1030	3.90×10^5	66 ± 4	NA	[56]
MoS_2 (72–74 L)	1030	1.89×10^4	− 250 ± 50	NA	[56]
MoS_2	1064	NA	− 3.8 ± 0.59	$(1.88 \pm 0.48) \times 10^{-3}$	[57]
WS_2 (1–3 L)	515	5.18×10^6	$(-2.9 \pm 1.0) \times 10^4$	NA	[56]
WS_2	800	8.88 nm^{-1}	$(-3.7 \pm 0.28) \times 10^5$	8.1 ± 0.41	[58]
WS_2 (1–3 L)	800	1.08×10^6	525 ± 205	NA	[56]
WS_2 (18–20 L)	800	7.22×10^5	− 397 ± 40	NA	[56]
WS_2 (1–3 L)	1030	7.17×10^5	$(1.0 \pm 0.8) \times 10^4$	NA	[56]
WS_2 (18–20 L)	1030	5.98×10^5	$(3.28 \pm 0.11) \times 10^3$	NA	[56]
WS_2 (39–41 L)	1030	8.57×10^5	$(2.75 \pm 0.10) \times 10^3$	NA	[56]
WS_2	1064	NA	− 5.1 ± 0.26	$(5.83 \pm 0.18) \times 10^{-2}$	[57]
WSe_2	1064	NA	1.9 ± 0.57	− (2.4 ± 1.23)	[57]
$Mo_{0.5}W_{0.5}S_2$	1064	NA	$(1.91 \pm 0.78) \times 10$	$-(8.73 \pm 1.47) \times 10^{-2}$	[57]
$MoTe_2$	800	NA	-7.4×10^5	− 1.24	[59]
$SnSe_2$	1030	NA	− 13,596	NA	[60]
$ReSe_2$	1560	0.25×10^3	$-(5.67 \pm 0.35) \times 10^3$	$-(2.81 \pm 0.13) \times 10^{-2}$	[34]
$ReSe_2$	1900	1.73×10^3	-13.8×10^3	-6.3×10^{-2}	This work

Table 1. Comparison of the nonlinear optical parameters of various TMDCs. *NA* not available.

reported that the nonlinear absorption coefficient and nonlinear refractive index of $ReSe_2$ are ~ -5.67×10^3 cm/GW and ~ -2.81×10^{-2} cm^2/GW at 1560 nm, respectively.

Fabrication of a $ReSe_2$/PVA-based saturable absorber. To determine the practicability of using $ReSe_2$ in a device at 1.9 μm, we fabricated a fiberized SA by dropping $ReSe_2$/PVA solution onto the surface of a side-polished SM2000 fiber and drying it for 1 day. The physical distance between the flat side and the fiber core was ~ 5 μm, while it had a side-polished section length of ~ 2 mm. After drying, we measured the insertion loss and polarization-dependent loss (PDL) (~ 3.4 dB and ~ 4 dB, respectively). It is possible to reduce the PDL by decreasing the polished section length of a side-polished fiber and/or increasing the distance between the core and the polished fiber surface[47,48], and thus we tried to use the aforementioned methods to reduce the PDL. However, we observed that the saturable absorption did not proceed very well due to reduced interaction between the deposited $ReSe_2$/PVA layer and the oscillating beam.

Next, we measured the nonlinear transmission of the $ReSe_2$/PVA-based SA versus the input beam peak power, for which a 1.9-μm thulium-holmium (Tm–Ho) co-doped fiber laser with a ~ 1.2-ps pulse width was used, as shown in the measurement setup in Fig. 7a. Figure 7b exhibits the measured transmission curve of the $ReSe_2$/PVA-based SA, from which the saturation intensity and modulation depth were estimated as ~ 11.4 MW/cm^2 and

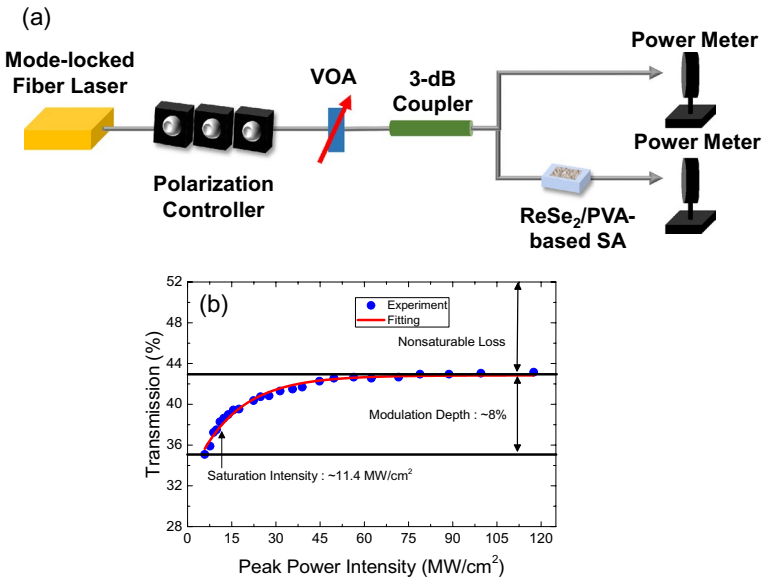

Figure 7. (**a**) Experimental setup for nonlinear transmission measurements and (**b**) the nonlinear transmission curve of the $ReSe_2$/PVA-based SA.

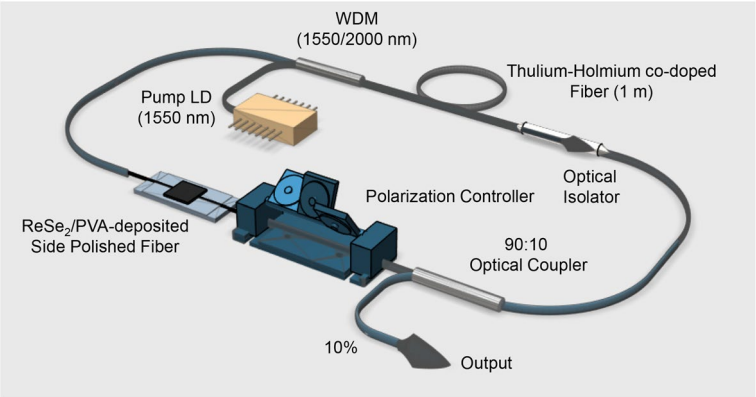

Figure 8. The fiber laser configuration and setup.

~ 8%, respectively. Hence, the measured modulation depth is high enough for mode-locking in an anomalously dispersive fiber cavity[49,50].

Fiber laser setup and results. The experimental setup of the fiber laser is illustrated in Fig. 8. The gain fiber was 1-m length of co-doped Tm-Ho fiber. Its peak absorption was ~ 13 dB/m at a wavelength of 1550 nm. The pumping source for the cavity was a 1550-nm pump laser diode and the pumping beam was launched into the Tm-Ho co-doped fiber through a 1550/2000 nm wavelength division multiplexer (WDM). A polarization controller (PC) was used to optimize the polarization state of the beam, while an isolator was placed in the cavity for unidirectional light propagation and the SA was inserted between the WDM and the PC. The output pulses were extracted through a 90:10 optical coupler.

Self-started optical pulses were induced at the pump power of ~ 224 mW. Our SA had a relatively high PDL, and so we believe that the mode-locking pulses were generated from the fiber laser cavity through the combined use of saturable absorption and NPR. The self-starting capability of our laser was tested by repeatedly increasing and decreasing the pump power near ~ 224 mW. The self-starting phenomenon was clearly observed, which we believed is due to the relatively slow response of the saturable absorption owing to the presence of $ReSe_2$. Anyhow, it is very difficult to negate the contribution of NPR to the laser mode-locking due to the 4 dB PDL value of the SA. Although it is difficult to realize self-starting mode-locking in fiber lasers with NPR mode-locking, it can be readily achieved in saturable absorption mode-locking. In this experiment, the self-starting operation was easily achieved without the necessity of a precise PC adjusting procedure. Therefore, we consider that the mode-locking demonstrated in this experiment is a hybrid type of saturable absorption and NPR.

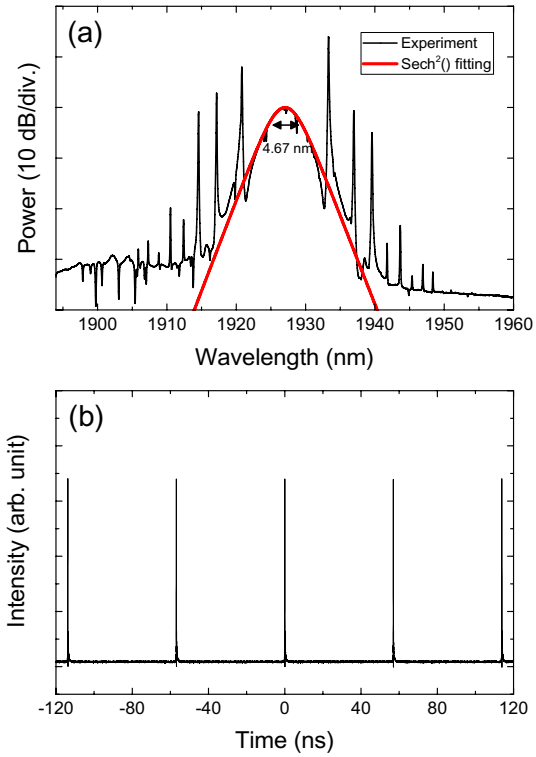

Figure 9. (**a**) An optical spectrum and (**b**) an oscilloscope trace of the output pulses at a pump power of ~ 297 mW.

The measured optical spectrum with its hyperbolic secant function curve is illustrated in Fig. 9a. The 3-dB bandwidth is ~ 4.67 nm with a center wavelength of ~ 1927 nm. Many Kelly sidebands were observed; it is well-known that these result from the periodic spectral interference of soliton pulses and dispersive waves in the laser cavity, depending on the phase-matching conditions. Therefore, it was possible to generate many Kelly sidebands when the phase-matching conditions were well satisfied in the laser cavity. Note that there are several reports on obtaining many Kelly peaks in passively mode-locked Tm-doped fiber lasers[51–53]. The temporal shape and spectrum of the output pulses exhibited little change when the pump power was changed from 224 to 297 mW. The measured period of the pulse train was ~ 56.92 ns (Fig. 9b) that corresponded to a repetition rate of ~ 17.57 MHz, which is a fundamental resonance frequency of the cavity.

We subsequently performed autocorrelation measurements of the output pulses (Fig. 10a), for which the output temporal width was measured at ~ 840 fs. Considering the 3-dB bandwidth of ~ 4.67 nm, the time-bandwidth product was calculated as ~ 0.317, which indicates that the pulses are almost transform-limited. Figure 10b depicts the radio frequency (RF) spectrum of the output pulses; the signal-to-noise ratio (SNR) was measured as ~ 62 dB with a fundamental frequency of ~ 17.57 MHz. A 1-GHz-span electrical spectrum was also measured (Fig. 10b), in which the strong harmonic signals imply that the laser output consisted of stable mode-locked pulses at the fundamental resonance frequency.

Figure 11a demonstrates the relationship between the average power of our laser output and the pump power, in which we can see the linear increase in output power with the increase in pump power. The maximum output power was ~ 12.7 mW, and the slope efficiency was ~ 1.5%. Stable output pulses existed at a pump power range from ~ 224 to ~ 297 mW.

Finally, the long-term stability of the pulse laser was examined by measuring the output spectrum every 10 min for 1 h with the pump power set at ~ 297 mW (Fig. 11b). It can be indirectly inferred from the measurements that stable mode-locking was maintained for the duration of the experiment.

Conclusion

We performed the Z-scan measurements at 1.9 μm to investigate the nonlinear optical responses in $ReSe_2$. From the results, the nonlinear absorption coefficient of $ReSe_2$ was approximately -11.3×10^3 cm/GW and the nonlinear refractive index was around -6.2×10^{-2} cm^2/GW. Furthermore, through energy band structure calculations with the PBE functional, we showed that the bandgap of $ReSe_2$ decreases with an increase in atomic defects, allowing for a broader saturable absorption bandwidth that can cover the mid-infrared wavelength region. Moreover, we experimentally demonstrated hybrid mode-locking with a 1.9-μm fiber laser with a $ReSe_2$/PVA-based SA. Due to both nonlinear saturable absorption and the high PDL of the prepared SA, 840-fs mode-locked pulses could be generated from a co-doped Tm-Ho fiber laser ring cavity.

We believe that this investigation will be technically meaningful from the viewpoint of providing useful data for producing promising nonlinear optical materials that could be used in the implementation of nonlinear

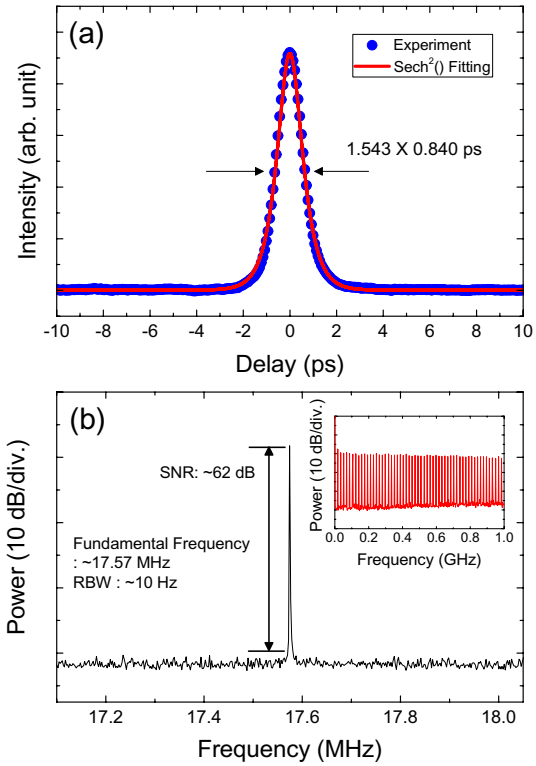

Figure 10. (**a**) An autocorrelation trace and (**b**) an electrical spectrum. Inset: the electrical spectrum over 1 GHz at a pump power of ~ 297 mW.

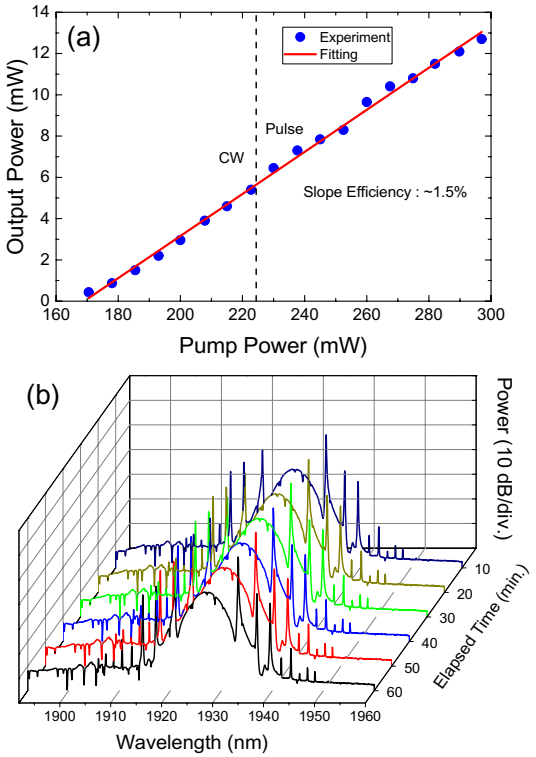

Figure 11. (**a**) Pump output characteristics with continuous wave and pulse regions shown. (**b**) Measured output optical spectrum with a pump power of ~ 297 mW for 1 h.

optical and photonic devices. Further investigations need to be conducted to fully understand the nonlinear optical properties of $ReSe_2$ in the mid-infrared spectral region beyond 2 μm.

Methods

Z-scan measurement. A 1.2-ps fiber laser operating at 1.9 μm was used as the input pulse. The input beam was focused through a plano-convex lens into the $ReSe_2$ sample, and the beam passing through the $ReSe_2$ sample was separated through a beam splitter. The sample was gradually moved in the propagation direction. One of the two separated beams was used for the OA Z-scan while the other passed through the aperture and was used for CA Z-scan. Power meters were used to measure the varying power of the beam while the sample moved.

Nonlinear transmission curve measurement. The fiber laser used in the Z-scan measurements was used as the input source that was adjusted using a variable optical attenuator. After a 3-dB coupler, the input pulses were separated into two ports. One was directly detected by a power meter to measure the reference beam power while the other was connected to an SA. Another power meter was connected to the prepared SA to monitor the output power for comparison with the input power. A PC was employed within the setup to show the non-negligible PDL of the SA.

Received: 24 December 2020; Accepted: 5 April 2021
Published online: 29 April 2021

References

1. Langrock, C., Kumar, S., McGeehan, J. E., Willner, A. E. & Fejer, M. M. All-optical signal processing using $\chi^{(2)}$ nonlinearities in guided-wave devices. *J. Lightwave Technol.* **24**, 2579–2592 (2006).
2. Li, L., Abdukerim, N. & Rochette, M. Mid-infrared wavelength conversion from As_2Se_3 microwires. *Opt. Lett.* **42**, 639–642 (2017).
3. Armstrong, D. J., Alford, W. J., Raymond, T. D., Smith, A. V. & Bowers, M. S. Parametric amplification and oscillation with walkoff-compensating crystals. *J. Opt. Soc. Am. B* **14**, 460–474 (1997).
4. Asobe, M., Kanamori, T. & Kubodera, K. Ultrafast all-optical switching using highly nonlinear chalcogenide glass fiber. *IEEE Photon. Technol. Lett.* **4**, 362–365 (1992).
5. Set, S. Y., Yaguchi, H., Tanaka, Y. & Jablonski, M. Laser mode locking using a saturable absorber incorporating carbon nanotubes. *J. Lightwave Technol.* **22**, 51–56 (2014).
6. Singer, K. D., Sohn, J. E. & Lalama, S. J. Second harmonic generation in poled polymer films. *Appl. Phys. Lett.* **49**, 248 (1986).
7. Petropouls, P. *et al.* 2*R*-regenerative all-optical switch based on a highly nonlinear holey fiber. *Opt. Lett.* **26**, 1233–1235 (2001).
8. Bao, Q. *et al.* Monolayer graphene as a saturable absorber in a mode-locked laser. *Nano Res.* **4**, 297–307 (2011).
9. Song, Y., Shi, X., Wu, C., Tang, D. & Zhang, H. Recent progress of study on optical solitons in fiber lasers. *Appl. Phys. Rev.* **6**, 021313 (2019).
10. Yan, Z. *et al.* Tunable and switchable dual-wavelength Tm-doped mode-locked fiber laser by nonlinear polarization evolution. *J. Lightwave Technol.* **24**, 1433–1439 (2006).
11. Li, J. *et al.* All-fiber passively mode-locked Tm-doped NOLM-based oscillator operating at 2-μm in both soliton and noisy-pulse regimes. *Opt. Express* **22**, 7875–7882 (2014).
12. Jin, X., Wang, X., Wang, X. & Zhou, P. Tunable multiwavelength mode-locked Tm/Ho-doped fiber laser based on a nonlinear amplified loop mirror. *Appl. Opt.* **54**, 8260–8264 (2015).
13. Zitter, R. N. Saturated optical absorption through band filling in semiconductors. *Appl. Phys. Lett.* **14**, 73 (1969).
14. Kieu, K. & Wise, F. W. Soliton thulium-doped fiber laser with carbon nanotube saturable absorber. *IEEE Photon. Technol. Lett.* **21**, 128–130 (2009).
15. Liu, X. & Cui, Y. D. Revealing the behavior of soliton buildup in a mode-locked fiber. *Adv. Photon.* **1**, 016003 (2019).
16. Wang, G. *et al.* Ultrafast nonlinear optical properties of a graphene saturable mirror in the 2 μm wavelength region. *Laser Photon. Rev.* **11**, 1700166 (2017).
17. Liu, M., Tang, R., Luo, A. P., Xu, W. C. & Luo, Z. C. Graphene-decorated microfiber knot as a broadband resonator for ultrahigh-repetition-rate pulse fiber lasers. *Photon. Res.* **6**, C1–C7 (2018).
18. Chen, S. *et al.* Broadband optical and microwave nonlinear response in topological insulator. *Opt. Express* **4**, 7875–7882 (2014).
19. Jhon, Y. I., Lee, J., Jhon, Y. M. & Lee, J. H. Topological insulators for mode-locking of 2-μm fiber lasers. *IEEE J. Sel. Top. Quantum Electron.* **24**, 1102208 (2018).
20. Zhang, H. *et al.* Molybdenum disulfide (MoS_2) as a broadband saturable absorber for ultra-fast photonics. *Opt. Express* **22**, 7249–7260 (2014).
21. Lee, J., Koo, J., Lee, J., Jhon, Y. M. & Lee, J. H. All-fiberized, femtosecond laser at 1912 nm using a bulk-like $MoSe_2$ saturable absorber. *Opt. Mater. Express* **7**, 2968–2979 (2017).
22. Huang, B. *et al.* Bulk-structured $PtSe_2$ for femtosecond fiber laser mode-locking. *Opt. Express* **27**, 2604–2611 (2019).
23. Li, L., Pang, L. H., Zhao, Q. Y., Liu, W. J. & Su, Y. L. VSe_2 nanosheets for ultrafast fiber lasers. *J. Mater. Chem. C* **8**, 1104–1109 (2020).
24. Liu, J.-S. *et al.* $SnSe_2$ nanosheets for subpicosecond harmonic mode-locked pulse generation. *Small* **15**, 1902811 (2019).
25. Feng, J. *et al.* 2D ductile transition metal chalcogenides (TMCs): Novel high-performance Ag_2S nanosheets for ultrafast photonics. *Adv. Opt. Mater.* **8**, 1901762 (2020).
26. Zhang, Y. *et al.* PbS nanoparticles for ultrafast pulse generation in optical communication region. *Part. Part. Syst. Charact.* **35**, 1800341 (2018).
27. Jhon, Y. I. *et al.* Metallic MXene saturable absorber for femtosecond mode-locked lasers. *Adv. Mater.* **29**, 1702496 (2017).
28. Jiang, X. *et al.* Broadband nonlinear photonics in few-layer MXene $Ti_3C_2T_x$ (T = F, O, or OH). *Laser Photon. Rev.* **12**, 1700229 (2018).
29. Feng, T. *et al.* MXene: Two dimensional inorganic compounds, for generation of bound state soliton pulses in nonlinear optical system. *Nanophotonics* **9**, 2505–2513 (2020).
30. Cui, Y., Lu, F. & Liu, X. Nonlinear saturable and polarization-induced absorption of rhenium disulfide. *Sci. Rep.* **7**, 40080 (2017).
31. Su, X. *et al.* Broadband rhenium disulfide optical modulator for solid-state lasers. *Photon. Res.* **6**, 498–505 (2018).
32. Du, L. *et al.* Few-layer rhenium diselenide: An ambient-stable nonlinear optical modulator. *Opt. Mater. Express* **8**, 926–935 (2018).
33. Li, Z. *et al.* Invited article: Mode-locked waveguide lasers modulated by rhenium diselenide: As a new saturable absorber. *APL Photon.* **3**, 080802 (2018).
34. Lee, L., Lee, K., Kwon, S., Soo, B. & Lee, J. H. Investigation of nonlinear optical properties of rhenium diselenide and its application as a femtosecond mode-locker. *Photon. Res.* **7**, 984–993 (2019).

35. Corbet, C. M., Sonde, S. S., Tutuc, E. & Benerjee, S. K. Improved contact resistance in $ReSe_2$ thin film field-effect transistors. *Appl. Phys. Lett.* **108**, 162104 (2016).
36. Qi, F. *et al.* Self-assembled chrysanthemum-like microspheres constructed by few-layer $ReSe_2$ nanosheets as a highly efficient and stable electrocatalyst for hydrogen evolution reaction. *Electrochim. Acta* **224**, 593–599 (2017).
37. Wolverson, D., Crampin, S., Kazei, A. S., Ilie, A. & Bending, S. J. Raman spectra of monolayer, few-layer, and bulk $ReSe_2$: An anisotropic layered semiconductor. *ACS Nano* **8**, 11154–11164 (2014).
38. Yang, S. *et al.* Layer-dependent electrical and optoelectronic responses of $ReSe_2$ nanosheet transistors. *Nanoscale* **6**, 7226–7231 (2014).
39. Jiang, S. *et al.* Application of chemical vapor-deposited monolayer $ReSe_2$ in the electrocatalytic hydrogen evolution reaction. *Nano Res.* **11**, 1787–1797 (2018).
40. Virtual Lab. Inc. *Materials Square* (2017). https://www.materialssquare.com/
41. Liu, F. *et al.* Optoelectronic properties of atomically thin ReSSe with weak interlayer coupling. *Nanoscale* **8**, 5826 (2016).
42. Mao, D. *et al.* WS2 saturable absorber for dissipative soliton mode locking at 1.06 and 1.55 μm. *Opt. Express* **23**, 27509–27519 (2015).
43. Koo, J. *et al.* Near-infrared saturable absorption defective bulk-structured WTe_2 for femtosecond laser mode-locking. *Adv. Funct. Mater.* **26**, 7454–7461 (2016).
44. Sheik-Bahae, M., Said, A. A. & Van Stryland, E. W. High-sensitivity, single-beam n_2 measurements. *Opt. Lett.* **14**, 955–957 (1989).
45. Ge, Y. *et al.* Broadband nonlinear photoresponse of 2D TiS_2 for ultrashort pulse generation and all-optical thresholding devices. *Adv. Opt. Mater.* **6**, 1701166 (2018).
46. Jiang, X. *et al.* Ultrathin metal-organic framework: and emerging broadband nonlinear optical material for ultrafast photonics. *Adv. Opt. Mater.* **6**, 1800561 (2018).
47. Zapata, J. D. *et al.* Efficient graphene saturable absorbers on D-shaped optical fiber for ultrashort pulse generation. *Sci. Rep.* **6**, 20644 (2016).
48. Kowalczyk, M. *et al.* Sb_2Te_3-deposited D-shaped fiber as a saturable absorber for mode-locked Yb-doped fiber lasers. *Opt. Mater. Express* **6**, 2273–2282 (2016).
49. Jeon, J., Lee, J. & Lee, J. H. Numerical study on the minimum modulation depth of a saturable absorber for stable fiber laser mode locking. *J. Opt. Soc. Am. B* **32**, 31–37 (2015).
50. Lee, J., Kwon, S. & Lee, J. H. Numerical investigation of the impact of the saturable absorber recovery time on the mode-locking performance of fiber lasers. *J. Lightwave Technol.* **38**, 4124–4132 (2020).
51. Qiangsong, J. *et al.* Mode-locking thulium-doped fiber laser with 1.78-GHz repetition rate based on combination of nonlinear polarization rotation and semiconductor saturable absorber mirror. *IEEE Photon. J.* **9**, 1502808 (2017).
52. Wang, P., Xiao, X., Grelu, P. & Yang, C. Subsideband generation associated with period-N pulsations in Tm soliton fiber lasers. *IEEE Photon. J.* **9**, 1502908 (2017).
53. Wang, T. *et al.* Passively mode-locked fiber lasers based on nonlinearity at 2-μm band. *IEEE J. Sel. Top. Quantum Electron.* **24**, 1102011 (2018).
54. Zhang, J. *et al.* Ultrafast saturable absorption of MoS_2 nanosheets under different pulse-width excitation conditions. *Opt. Lett.* **43**, 243–246 (2018).
55. He, M. *et al.* Enhanced nonlinear saturable absorption of MoS_2/graphene nanocomposite films. *J. Phys. Chem. C* **121**, 27147–27153 (2017).
56. Zhang, S. *et al.* Direct observation of degenerate two-photon absorption and its saturation in WS_2 and MoS_2 monolayer and few-layer films. *ACS Nano* **9**, 7142–7150 (2016).
57. Bikorimana, S. *et al.* Nonlinear optical response in two-dimensional transition metal dichalcogenide multilayer: WS_2, WSe_2, MoS_2 and $Mo_{0.5}W_{0.5}S_2$. *Opt. Express* **24**, 20685–20695 (2016).
58. Zheng, X. *et al.* Z-scan measurement of the nonlinear refractive index of monolayer WS_2. *Opt. Express* **23**, 15616–15623 (2015).
59. Wang, J. *et al.* Mode-locked thulium-doped fiber laser with chemical vapor deposited molybdenum ditelluride. *Opt. Lett.* **43**, 1998–2001 (2018).
60. Cheng, C. *et al.* Tin diselenide as a new saturable absorber for generation of laser pulses at 1 μm. *Opt. Express* **25**, 6132–6140 (2017).

Acknowledgements

This work was supported by Basic Science Research Program through the National Research Foundation of Korea (NRF) funded by the Ministry of Science and ICT, (2021R1A2C1004988), Republic of Korea for Jinho Lee. This work was supported by the Basic Study and Interdisciplinary R&D Foundation Fund of the University of Seoul (2020) for Ju Han Lee.

Author contributions

J.L. and J.H.L. conceived the idea of the experiment, J.L. and S.K. conducted the measurements, J.L. performed the numerical simulations. JL., T.K., L.Z. and J.J. analyzed the results, J.L. and J.H.L. wrote the manuscript. All authors reviewed the manuscript.

Competing interests

The authors declare no competing interests.

Additional information

Correspondence and requests for materials should be addressed to J.H.L.

Reprints and permissions information is available at www.nature.com/reprints.

Publisher's note Springer Nature remains neutral with regard to jurisdictional claims in published maps and institutional affiliations.